



Chapter 4

The Experimental Method

4.1 Overview

Two Coulomb excitation experiments [25, 26] were performed at Helmholtzzentrum für Schwerionenforschung GSI, Darmstadt (Germany) [27] and Inter University Accelerator Centre IUAC, New Delhi (India) [28] to investigate the different tin isotopes. Fig 4.1 shows the pictures of the particle- γ coincidence set-up at GSI and at IUAC.

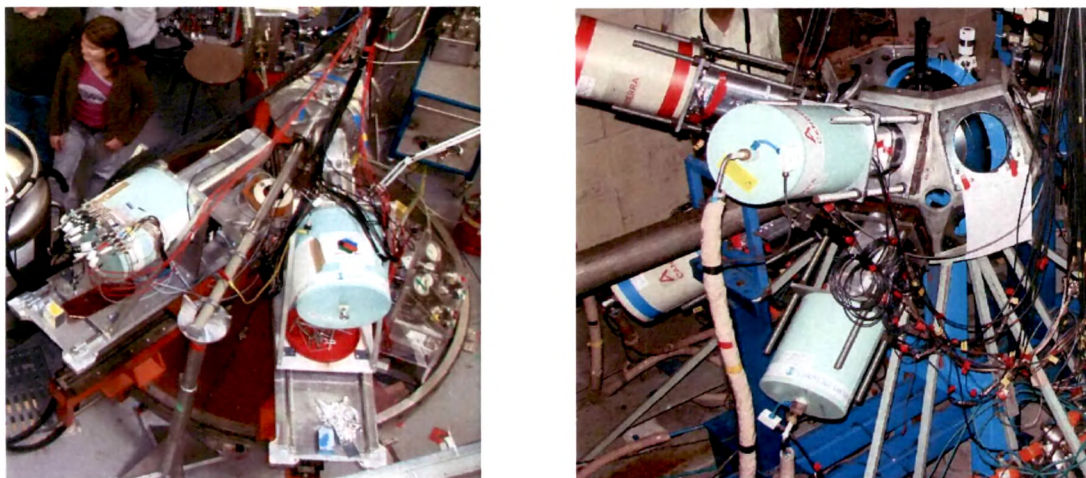


Figure 4.1: Particle- γ coincidence set-up at GSI (left) and at IUAC (right).

At GSI we performed two consecutive measurements using ^{114}Sn and ^{116}Sn beams at an energy of 3.4A MeV on a ^{58}Ni target. The tin beams were provided by the UNILAC accelerator at GSI. Beam particles were incident on a $0.7\text{mg}/\text{cm}^2$ ^{58}Ni target with a purity of 99.9%. In the experiment carried out at IUAC, targets of ^{112}Sn and ^{116}Sn were bombarded with ^{58}Ni beam at 175 MeV using a tandem Van de Graaf accelerator. Both targets were of thickness $0.53\text{mg}/\text{cm}^2$ with an enrichment of 99.5% and 98%, respectively. In both cases the bombarding energy was well below the safe bombarding energy [see chapter 3].

The scattered beam particles and recoils were detected in an annular gas-filled parallel plate avalanche counter PPAC [29, 30], subtending the angular range 15° to 45° in the forward direction. De-excitation γ -rays emitted after Coulomb excitation were measured with two Super-Clover (Ge) detectors [31] mounted at forward direction (GSI) and four Clover(Ge) detectors [31] mounted at backward direction (IUAC), respectively. The schematic view of the experiment performed at IUAC is shown in fig. 4.2.

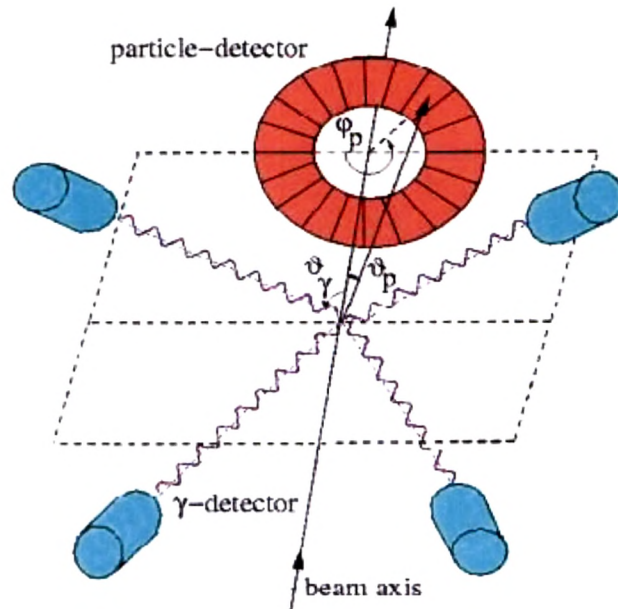


Figure 4.2: Schematic view of the experiment performed at IUAC. A position sensitive annular gas-filled parallel plate avalanche counter (PPAC) was placed in forward direction covering the angular range of $15^\circ \leq \vartheta_{lab} \leq 45^\circ$. Four Clover detectors were mounted at $\vartheta_\gamma \sim 135^\circ$ with respect to the beam direction.

The PPAC was position-sensitive in both the azimuthal φ and the polar ϑ angles. The azimuthal angle φ was obtained from the anode foil which was divided into 20 radial sections of 18° each. In order to measure the polar angle, ϑ , the cathode was patterned in concentric conductor rings of constant $\tan\vartheta$, each 1mm wide, with an insulating gap of 0.5mm between them. Each ring was connected to its neighbour by a delay-line of 2ns per tap. The cathode signals were read out from the innermost and outermost rings, and the ϑ information was derived from the time difference of the anode and cathode signals. The scattering angle ϑ is

related to the delay line signals by

$$\tan\vartheta \approx \text{delay inner contact} - \text{delay outer contact} \quad (4.1)$$

It can be calibrated by the boundaries of the PPAC using the following linear equation.

$$\tan\vartheta = \frac{\tan 45^\circ - \tan 15^\circ}{ch_2 - ch_1} \cdot (ch - ch_1) + \tan 15^\circ \quad (4.2)$$

In both experiments Clover Germanium (Ge) detectors were used to measure the de-excited gamma rays. Each Clover detector consists of four coaxial N-type Ge crystals arranged like a four leaf clover. At GSI two Super-Clover Ge-detectors were mounted at angles of $\vartheta_\gamma = 25^\circ$ relative to the beam axis in the forward direction at a distance of 20 cm from the target. Each Germanium crystal had a length of 140 mm and a square front face with two flat parts at 90° along the whole length and two tapered parts at an angle of 15° . The front sides of the Super-clover detectors were covered by a stacked shielding of 0.2mm Ta, 1.0mm Sn, and 0.5mm Cu plates. The addback factor of Super Clovers at 1.3 MeV was 1.3. At IUAC the Ge crystals dimensions were 80cm in diameter and 80cm in length. The four Clover detectors (distance to target 22 ± 2 cm) were mounted at $\vartheta_\gamma \sim 135^\circ$ with respect to the beam direction. The φ_γ -angles for the Clover detectors were $\pm 55^\circ$ and $\pm 125^\circ$ with respect to the vertical direction (see fig. 4.2). Low energy radiations were suppressed by using Cu, Sn and Pb absorbers of thickness between 0.5 mm and 0.7 mm placed in front of Clover detectors. The addback factor for the Clovers was 1.5 for a γ -ray energy of 1MeV.

4.2 Kinematics and Particle Identification

In the following, the kinematics for both experiments will be discussed. The data are displayed in the fig. 4.3 for the Coulomb excitation performed at GSI (left) and at IUAC (right). The kinetic energies of both reaction partners are displayed as a function of the centre-of-mass (c.m) scattering angle (θ_{cm}) and the scattering angles in the laboratory frame for the recoil nucleus (ϑ_4) and the projectile (ϑ_3), respectively. In both the cases the scattered particles are detected in the angular range between 15° and 45° in laboratory frame.

For Sn beams (GSI) kinematical correlations were used to discriminate between target nuclei and projectiles. The used parallel plate avalanche counter (PPAC) was placed 13cm downstream of the target and splitted into two independent parts, in a left (L) and a right (R) half. The flight time difference ΔTOF was measured between L and R. If the projectile (particle-3) is detected in the left half, then ϑ_3 is plotted versus $t_3 - t_4$ in the correlation diagram. In case of a detected target nucleus in the left half, ϑ_4 is plotted versus $t_4 - t_3$. In this way one obtains the theoretical plot which can be compared with the experimental data in fig. 4.4. The figure presents data from the ^{116}Sn beam striking on the ^{58}Ni target as an example.

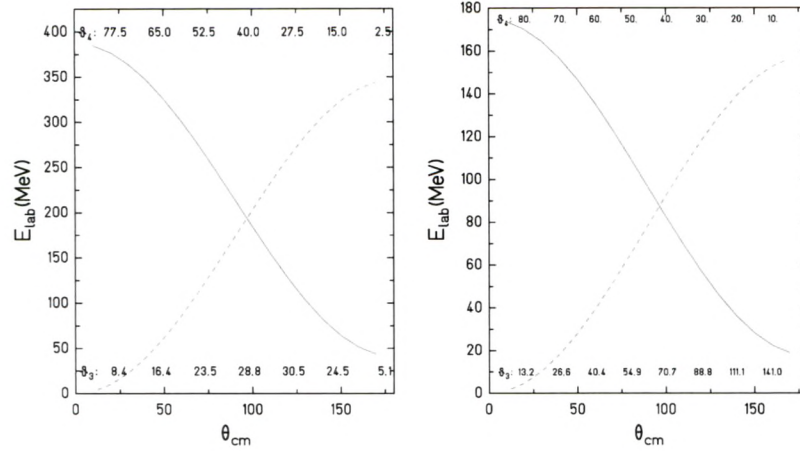


Figure 4.3: Kinematics of Coulomb excitation experiments with ^{114}Sn beam on ^{58}Ni target (left) and with ^{58}Ni beam on ^{112}Sn target (right). Energy dependence of both reaction partners is plotted as a function of the scattering angle in the centre of mass system (θ_{cm}) and laboratory frame (ϑ_3, ϑ_4). Solid lines correspond to projectile-like fragment and the dashed lines correspond to target-like fragments.

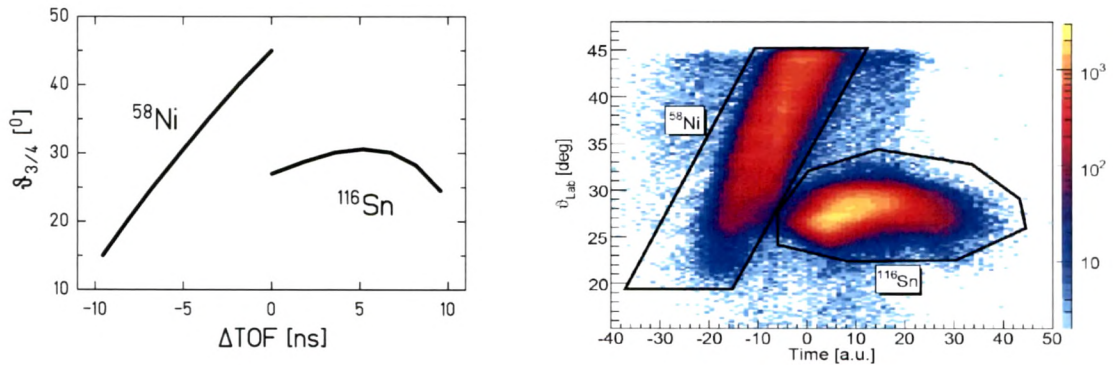


Figure 4.4: Scattered projectiles and target nuclei coincidences were detected in the PPAC for the ^{116}Sn beam incident on the ^{58}Ni target. The scattering angle is plotted versus the flight time differences of both reaction partners. The corresponding kinematical cuts applied for coincident γ -rays are indicated. See text for details.

For the Sn projectiles there exists a maximum kinematical angle given by

$$\vartheta_{max} = \arcsin \frac{A_2}{A_1} \quad (4.3)$$

yielding a value of $\vartheta_{max}=30.0^\circ(30.6^\circ)$ for the system $^{116}\text{Sn}(^{114}\text{Sn})+^{58}\text{Ni}$. Fig. 4.4 demonstrates the unambiguous identification of projectile and target nucleus and the assignment of the corresponding scattering angle θ_{cm} . For ejectiles detected in the PPAC, the corresponding scattering angles of ^{114}Sn and ^{116}Sn varied between $24^\circ \leq \vartheta_{lab} \leq 31^\circ$.

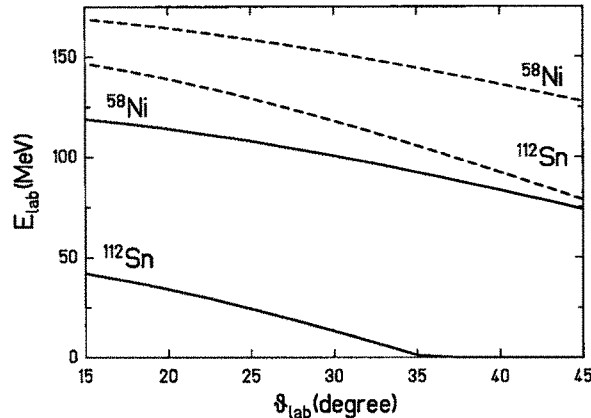


Figure 4.5: Kinetic energies of the scattered ^{58}Ni projectiles and ^{112}Sn recoils detected in the angular range of 15° to 45° covered by the PPAC. The dashed lines are based on two body kinematics for a beam energy of 175 MeV, while full lines are corrected for energy loss [32] in a $10\ \mu\text{m}$ MYLAR foil, which was used as entrance window of the PPAC.

For the measurement performed at IUAC only one particle, the projectile or the recoil, was detected in the sensitive angular range. Therefore ΔTOF measurements were not possible. However, the differential energy loss $\frac{dE}{dX}(Z=28) \neq \frac{dE}{dX}(Z=50)$ allowed to suppress one reaction partner. An entrance window of $10\ \mu\text{m}$ thick MYLAR foil was used for the particle counter which reduced the kinetic energy of both reaction partners (see fig. 4.5). The energy loss in MYLAR ($\rho=1.39\ \text{g}/\text{cm}^3$) was taken from Northcliff and Schilling [32]. While the ^{58}Ni projectiles could still be measured in the PPAC, the Sn recoils were either stopped in the entrance window or were close to the detection limit (for details of the analysis see chapter 5). In this way distant collisions (Ni detected in PPAC) could be selected for the analysis.

4.3 Electronics

Both data acquisition (DAQ) systems for the experiments performed at GSI and IUAC were very similar. During the IUAC experiment, 16 energies from the four Clover detectors, four timing signals from the Clover, 20 timing signals from individual front PPAC detectors, and four signals from the two ends of the delay lines were recorded event by event. Energy and time signals were taken from each Ge crystal and the pulse processing was carried out using

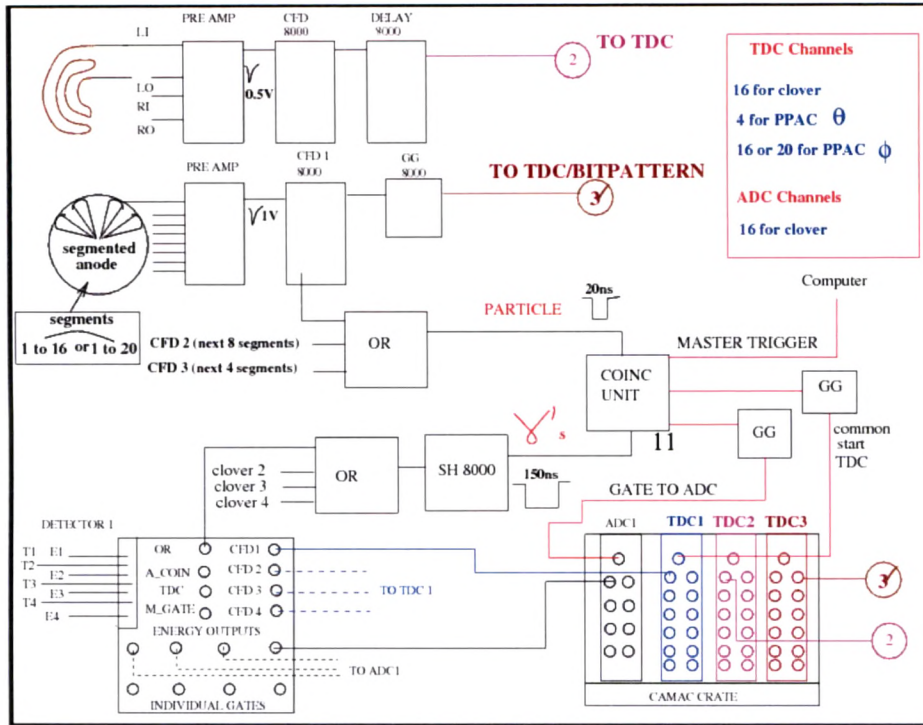


Figure 4.6: Block diagram showing the electronics used for the Coulomb excitation experiments at IUAC. (CFD: constant fraction discriminator, SH: shaper, GG: gate generator, A(T)DC: analog-(time)-to-digital-converter).

special Clover electronic modules [33, 34]. This double width NIM module replaces various electronics modules necessary to operate a Clover detector. It consists of four spectroscopic amplifiers of $3\mu\text{s}$ shaping time, five timing filter amplifiers (TFA), five constant fraction discriminator (CFD), five gate generators (GG) and one coincidence unit. The performance of this special electronic module with respect to conventional electronics was tested with a Super-Clover detectors at GSI and the results are summarized in the following paper [35]. For the PPAC standard NIM modules were used with the following CFD settings: fraction=0.2 (0.4) and delay=6ns(18ns) for the anode segments and the delay lines, respectively. All this is depicted in the schematic diagram of the Coulomb excitation DAQ system shown in fig. 4.6.

All time and energy signals were read out for the following two trigger conditions:

- i) particle signals registered in the annular counter, as a measure of the beam intensity, and
- ii) particle- γ coincidences measured with the annular counter and one of the Ge crystals.

In order to avoid any systematic error due to instrumental drift, runs from ^{112}Sn and ^{116}Sn targets, each of ~ 3 hours duration, were interspersed alternatively.

Energy and efficiency calibration run for the Clover detectors was carried out at the end of experiment using a ^{152}Eu source.

The raw γ -ray spectrum from a Clover detector in coincidence with the scattered projectile is shown in fig. 4.7. It shows the background radiation (narrow peaks) and the broad distributions as of the Doppler shifted γ -radiation from the scattered projectiles (~ 1430 keV) and the target recoils (~ 1225 keV). The shifted energy E_γ is strongly dependent on the ion velocity and on the relative angle between the particle and Ge detector. The velocities of both scattered projectiles and target recoil could be calculated from the measured scattering angle using two-body kinematics.

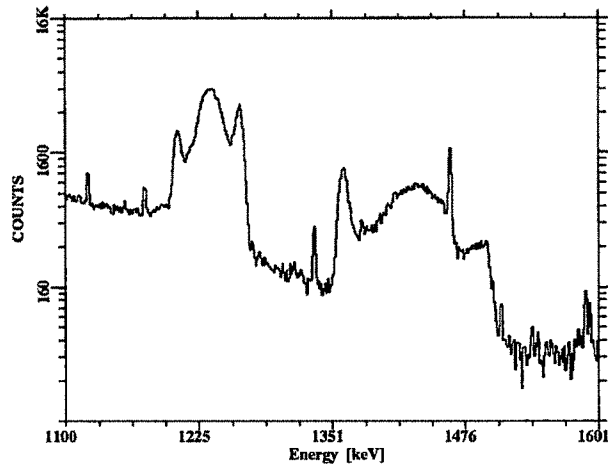


Figure 4.7: Ungated γ -ray spectrum from Clover-2 detector (IUAC experiment) in coincidence with scattered projectiles measured in the particle detector.

4.4 Doppler Correction

If a nucleus emits a γ -ray of energy $E_{\gamma 0}$ while it is moving with a velocity v_i at a relative angle $\vartheta_{\gamma i}$ between the γ -emission and the particle direction, the measured energy E_γ is Doppler shifted. Therefore, Doppler shift corrections were performed for both experiments at GSI and IUAC. We distinguish four different cases for projectile and target excitation and the detection of either the projectile or target nucleus. In the following, A_1 , Z_1 and A_2 , Z_2 are the mass (in amu) and charge number of the projectile and target nucleus, respectively, and E_{lab} is the lab-energy of the projectile (in MeV). (The subscript i is used with the convention $i = 1$ for projectile and $i = 2$ for target excitation). The velocity of the centre of mass (c.m) system is given by (all velocities are in units of the velocity of light)

$$v_{cm} = 0.04634 \cdot \left(1 + \frac{A_2}{A_1}\right)^{-1} \sqrt{\frac{E_{lab}}{A_1}} \quad (4.4)$$

CASE 1: Projectile measured with PPAC and projectile excitation

The scattering angle of the projectile in the c.m. system is given by

$$\theta_{cm} = \vartheta_1 + \arcsin\left(\frac{A_1}{A_2} \sin\vartheta_1\right) \quad (4.5)$$

and allows the calculation of the velocity of the excited nucleus in the laboratory system

$$v_1 = v_{cm} \cdot \left[1 + \left(\frac{A_2}{A_1}\right)^2 + 2 \cdot \left(\frac{A_2}{A_1}\right) \cdot \cos\theta_{cm} \right]^{\frac{1}{2}} \quad (4.6)$$

The correlation angle $\vartheta_{\gamma 1}$ can be calculated from the γ -emission angles $(\vartheta_\gamma, \varphi_\gamma)$ in the laboratory frame by

$$\cos\vartheta_{\gamma 1} = \cos\vartheta_\gamma \cdot \cos\vartheta_1 + \sin\vartheta_\gamma \cdot \sin\vartheta_1 \cdot \cos(\varphi_\gamma - \varphi_1) \quad (4.7)$$

with

$$\cos(\varphi_\gamma - \varphi_1) = \cos\varphi_\gamma \cdot \cos\varphi_1 + \sin\varphi_\gamma \cdot \sin\varphi_1 \quad (4.8)$$

The unshifted γ -ray energy $E_{\gamma 0}$ is calculated from the measured energy E_γ by

$$\frac{E_{\gamma 0}}{E_\gamma} = \frac{1 - v_1 \cdot \cos\vartheta_{\gamma 1}}{\sqrt{1 - v_1^2}} \quad (4.9)$$

CASE 2: Projectile measured with PPAC and target excitation

The recoil angle can be calculated by using eq. 4.5

$$\vartheta_2 = 0.5 \cdot (180^\circ - \theta_{cm}) \quad (4.10)$$

which allows the determination of the recoil velocity by

$$v_2 = 2 \cdot v_{cm} \cdot \cos\vartheta_2 \quad (4.11)$$

The correlation angle $\vartheta_{\gamma 2}$ can be calculated from the γ -emission angles $(\vartheta_\gamma, \varphi_\gamma)$ in the laboratory frame by

$$\cos\vartheta_{\gamma 2} = \cos\vartheta_\gamma \cdot \cos\vartheta_2 - \sin\vartheta_\gamma \cdot \sin\vartheta_2 \cdot \cos(\varphi_\gamma - \varphi_1) \quad (4.12)$$

with

$$\cos(\varphi_\gamma - \varphi_1) = \cos\varphi_\gamma \cdot \cos\varphi_1 + \sin\varphi_\gamma \cdot \sin\varphi_1 \quad (4.13)$$

The Doppler shift correction is done by the following formulae

$$\frac{E_{\gamma 0}}{E_\gamma} = \frac{1 - v_2 \cdot \cos\vartheta_{\gamma 2}}{\sqrt{1 - v_2^2}} \quad (4.14)$$

CASE 3: Target nucleus measured with PPAC and target excitation

From the measured scattering angle ϑ_2 the recoil velocity can be calculated by

$$v_2 = 2 \cdot v_{cm} \cdot \cos\vartheta_2 \quad (4.15)$$

The correlation angle $\vartheta_{\gamma 2}$ can be calculated from the γ -emission angles $(\vartheta_\gamma, \varphi_\gamma)$ in the laboratory frame by

$$\cos\vartheta_{\gamma 2} = \cos\vartheta_\gamma \cdot \cos\vartheta_2 + \sin\vartheta_\gamma \cdot \sin\vartheta_2 \cdot \cos(\varphi_\gamma - \varphi_2) \quad (4.16)$$

with

$$\cos(\varphi_\gamma - \varphi_2) = \cos\varphi_\gamma \cdot \cos\varphi_2 + \sin\varphi_\gamma \cdot \sin\varphi_2 \quad (4.17)$$

The Doppler shift correction is done by the following formulae

$$\frac{E_{\gamma 0}}{E_\gamma} = \frac{1 - v_2 \cdot \cos\vartheta_{\gamma 2}}{\sqrt{1 - v_2^2}} \quad (4.18)$$

CASE 4: Target nucleus measured with PPAC and projectile excitation

The c.m. angle can be calculated from the recoil angle in the laboratory frame

$$\theta_{cm} = 180^\circ - 2 \cdot \vartheta_2 \quad (4.19)$$

This allows the determination of the recoil velocity by

$$v_1 = v_{cm} \cdot \left[1 + \left(\frac{A_2}{A_1} \right)^2 + 2 \cdot \left(\frac{A_2}{A_1} \right) \cdot \cos\theta_{cm} \right]^{\frac{1}{2}} \quad (4.20)$$

The scattering angle ϑ_1 can be calculated by

$$\cos\vartheta_1 = \frac{v_{cm}}{v_1} \left(1 + \frac{A_2}{A_1} \cdot \cos\theta_{cm} \right) \quad (4.21)$$

The correlation angle $\vartheta_{\gamma 1}$ can be calculated from the γ -emission angles $(\vartheta_\gamma, \varphi_\gamma)$ in the laboratory frame by

$$\cos\vartheta_{\gamma 1} = \cos\vartheta_\gamma \cdot \cos\vartheta_1 - \sin\vartheta_\gamma \cdot \sin\vartheta_1 \cdot \cos(\varphi_\gamma - \varphi_2) \quad (4.22)$$

with

$$\cos(\varphi_\gamma - \varphi_2) = \cos\varphi_\gamma \cdot \cos\varphi_2 + \sin\varphi_\gamma \cdot \sin\varphi_2 \quad (4.23)$$

The Doppler shift correction is done by the following formulae

$$\frac{E_{\gamma 0}}{E_\gamma} = \frac{1 - v_1 \cdot \cos\vartheta_{\gamma 1}}{\sqrt{1 - v_1^2}} \quad (4.24)$$

The Doppler correction is essential for reducing the often considerable Doppler broadening of the peaks. The fig. 4.8 shows the Doppler corrected γ -ray spectra measured at GSI for case 3 and case 4. Due to the PPAC polar angle resolution of 2° , the scattering angle of the projectile and, accordingly, the velocity were best determined by a reconstruction from the position information of the target nucleus (see fig. 4.4 with cuts on ^{58}Ni) and hence used for the Doppler correction. A γ -ray energy resolution of 0.7% (FWHM) was obtained for decays from projectile excitation and 1.0% (FWHM) for decays from target excitation. The difference was caused by the Doppler broadening due to the higher velocity of the latter particles.

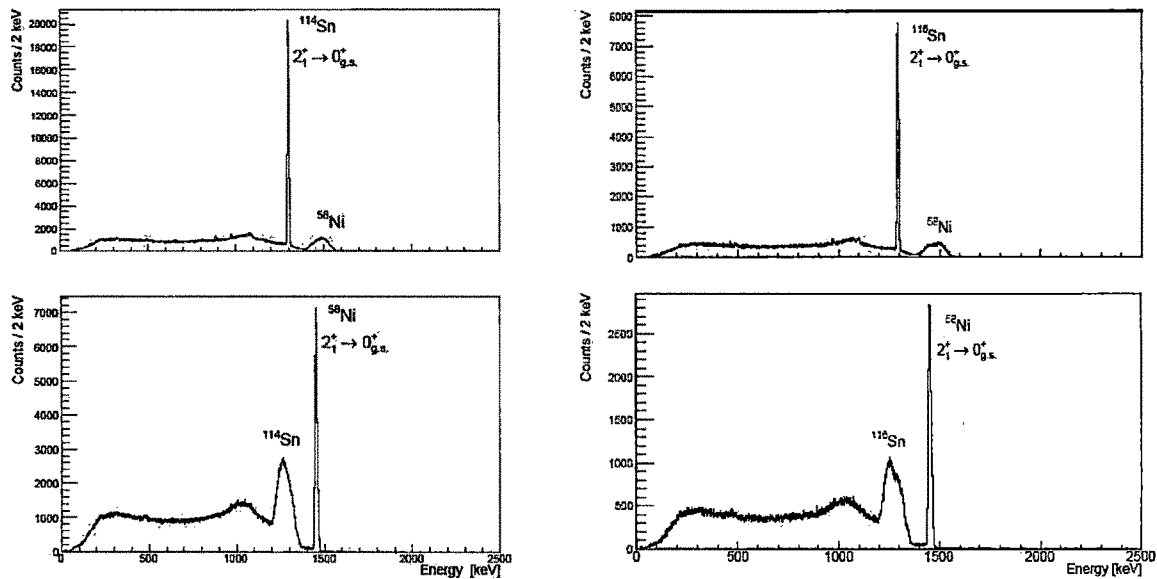


Figure 4.8: Doppler corrected γ -ray spectra associated with a coincidence of two particles in the PPAC. The Doppler correction (case 4) was applied using kinematical information of the target nuclei (^{58}Ni cuts in fig. 4.4), but assuming a projectile excitation of ^{114}Sn (left) and ^{116}Sn (right), respectively. The elevation between 1400keV and 1600keV corresponds to decays from the 2_1^+ state of the ^{58}Ni ejectiles. In order to obtain narrow peaks for the target excitation of ^{58}Ni , the same data were used but the Doppler correction (case 3) was applied to obtain the lower spectra.